ASME Journal of Heat and Mass Transfer
Online journal at:
https://asmedigitalcollection.asme.org/heattransfer

Analysis of Multilayer Cylindrical Thermal Conduction With a Time-Varying Convective Boundary Condition

Long Zhou
Department of Vehicle Engineering,
School of Mechanical and Power Engineering,
Henan Polytechnic University,
Jiaozuo, Henan 454003, China

Mohammad Parhizi
Electrochemical Safety Research Institute,
UL Research Institutes,
Houston, TX 77204

Ankur Jain[1]
Department of Mechanical and Aerospace Engineering,
University of Texas at Arlington,
Arlington, TX 76019
e-mail: jaina@uta.edu

Heat transfer in a multilayer body plays a key role in design and optimization of several engineering systems. While the analysis of simple multilayer problems is quite straightforward, realistic scenarios such as time-dependent boundary conditions result in significant complications in analysis. This work presents thermal analysis of a one-dimensional heat-generating multilayer cylinder with time-varying convective heat transfer at the boundary. Such a scenario may occur in applications such as nuclear reactors, jet impingement cooling, turbine blade heat transfer, as well as casting and related manufacturing processes. Analysis is presented for both annular and solid cylinders. A derivation for the temperature distribution is carried out, using a shifting function to split the time-dependent boundary condition into two parts, followed by appropriate mathematical substitution. For particular special cases, the analytical results derived here are shown to reduce exactly to results from past work. Good agreement of the theoretical results with numerical simulations is also demonstrated. Thermal response to various realistic time-dependent boundary conditions is analyzed. This work contributes towards the design of realistic multilayer problems and may facilitate the optimization of engineering systems where multilayer thermal conduction plays a key role.
[DOI: 10.1115/1.4063961]

Keywords: multilayer diffusion, convective boundary condition, thermal design, analytical modeling

1 Introduction

Heat transfer in multilayer structures plays a key role in several engineering systems. For example, semiconductor devices and systems are often multilayer in nature, and include heat generation and interfacial thermal resistance [1]. As another example, a nuclear fuel rod is often designed as a concentric multilayer cylinder, in which specific layers comprising the nuclear fuel generate heat. In addition, significant interfacial thermal resistance also often exists [2]. Other multilayer systems of relevance include insulation materials [3], aerospace vehicles [4], and biological systems [5]. Further, multilayer diffusive mass transfer is also important in engineering problems such as air pollution analysis [6] and drug delivery [7].

The safety and efficiency of engineering systems such as those cited above depend critically on understanding the nature of multilayer thermal transport in these systems. Both experimental and theoretical modeling approaches have been adopted in the past toward this goal. For example, thermal analysis of a three-dimensional integrated circuit (3D IC) has been presented [8,9] and used for designing effective thermal management approaches to minimize temperature rise [10]. Experimental methods have significant limitations in terms of the cost and time needed to set up and carry out measurements, particularly at the design stage, when quick exploration of a large parameter space is desirable. In contrast, theoretical and numerical models may facilitate the rapid prediction of temperature distribution. A key drawback of theoretical and numerical modeling is the uncertainty associated with values of thermal properties and other parameters, particularly when working on new materials.

Several papers have presented multilayer thermal conduction analysis under a variety of conditions. General solution procedures have been outlined in several papers and books [11–14], while solutions for specific problems have also been presented. Multilayer diffusion with convective cooling boundary conditions has received special attention in the literature. Such a boundary condition is able to model a variety of realistic problems. Most of the literature assumes that convective heat transfer conditions at the boundary do not change with time or space. For example, closed-form [15] and iterative [16] solution approaches based on this assumption have been presented for multilayer 3D ICs. Spatial variation of the convective heat transfer coefficient h in multilayer problems has been analyzed [17–19].

The convective heat transfer coefficient h in multilayer problems may often vary with time. Representative examples include the cooling of nuclear fuel rods [20], heat transfer due to pulsating flows [21], and jet impingement cooling [22], where switching the jet on and off results in a time-dependent h. Analysis of problems with

[1]Corresponding author.
Manuscript received March 9, 2023; final manuscript received October 5, 2023; published online November 30, 2023. Assoc. Editor: Timothy S. Fisher.

time-dependent h is much more complicated than with a constant h, or a space-dependent h. Numerical and analytical solutions of such time-dependent problems have been presented for a uniform, single-layer body. Techniques used in such papers include finite-differencing [23], Laplace transforms [24], shifting function method [25,26], and the use of time-dependent eigenvalues [27]. The latter approach, while powerful and versatile, suffers from challenges associated with eigenvalue computation.

Most of the literature cited above pertains only to a homogeneous, single-layer body. In comparison, only limited work has been presented for multilayer thermal conduction with time-dependent convective cooling at the boundary. A general procedure for such problems using the finite integral transform has been presented [13]. Specific solutions for two-layer bodies have been presented [3,28]. More recently, this problem has been solved for a multilayer Cartesian body [29]. The temperature field in this problem was derived using the shifting function method. It was shown that the general solution reduces correctly to well-known expressions for a homogeneous body.

Since similar problems occur in engineering problems involving cylinders as well, it is important to analytically derive the temperature field in a multilayer cylinder to account for a convective boundary condition that varies with time, i.e., $h(t)$. This paper addresses this problem and specifically derives an expression for the transient temperature field in a one-dimensional multilayer cylinder with a time-dependent convective heat transfer boundary condition. Thermal analysis of a multilayer solid cylinder is also presented. The transient temperature field is derived using the shifting function method [25] and the orthogonal expansion method [14,30,31]. The general results derived here are shown to reduce to previously reported results pertaining to simplified special cases and also agree well with finite-element computation. Results derived here are used to analyze the impact of various forms of $h(t)$ on the temperature distribution. This work advances the fundamental understanding of multilayer thermal conduction and may help design and optimize a variety of multilayer engineering devices and systems.

2 Analytical Modeling

2.1 Problem Definition. The problem of interest in this work comprises a one-dimensional M-layer, annular cylinder as shown in Fig. 1(*a*). Each layer has a thickness of $(r_i - r_{i-1})$ (m), while the inner radius of the annulus is r_0 (m). Each layer generates heat $Q_i(r,t)$ ($\mathrm{Wm^{-3}}$) that may vary with space and time. Heat transfer at the inner and outer boundaries is modeled by constant and time-dependent convective heat transfer coefficients h_1 ($\mathrm{Wm^{-2}K^{-1}}$) and $h_M(t)$ ($\mathrm{Wm^{-2}K^{-1}}$), respectively. Thermal conductivity and diffusivity of the ith layer are denoted by k_i ($\mathrm{Wm^{-1}K^{-1}}$) and α_i ($\mathrm{m^2s^{-1}}$), respectively. All properties are assumed to be constant and uniform. R_i ($\mathrm{Km^2W^{-1}}$) denotes the interfacial thermal contact resistance between adjacent layers, as shown in Fig. 1(*a*). The initial temperature field in the cylinder is denoted by $T_{\mathrm{in}}(r)$ (K). The goal of the analysis is to derive an expression for the transient temperature rise distribution $T_i(r,t)$ (K) in each layer of the cylinder. While Fig. 1(*a*) shows the annular multilayer cylinder problem, a similar problem involving a multilayer solid cylinder, shown in Fig. 1(*b*) is also considered here.

2.2 Annular Cylinder. Based on the problem definition and assumptions listed above, the governing differential equation for the ith layer of the multilayer cylinder may be written as

$$\frac{1}{\alpha_i}\frac{\partial T_i}{\partial t} = \frac{\partial^2 T_i}{\partial r^2} + \frac{1}{r}\frac{\partial T_i}{\partial r} + \frac{Q_i(r,t)}{k_i} \tag{1}$$

for $i = 1,2,\ldots,M$.

The following boundary and initial conditions apply

$$T_i(r,t) = T_{\mathrm{in}}(r) \qquad (t=0) \tag{2}$$

$$k_1\frac{\partial T_1}{\partial r} = h_1 T_1 \qquad (r = r_0) \tag{3}$$

$$-k_M\frac{\partial T_M}{\partial r} = h_M(t) T_M \qquad (r = r_M) \tag{4}$$

At each interface, the heat flux out of one layer must equal heat flux into the adjacent layer. Additionally, the interfacial thermal resistance may be used to write a relationship between interfacial temperatures in the two layers, i.e.

$$T_{i-1}(r,t) = T_i(r,t) - k_i R_i\frac{\partial T_i}{\partial r} \quad (r = r_{i-1};\ i = 2,3,\ldots,M) \tag{5}$$

$$k_{i-1}\frac{\partial T_{i-1}}{\partial r} = k_i\frac{\partial T_i}{\partial r} \qquad (r = r_{i-1};\ i = 2,3,\ldots,M) \tag{6}$$

The following nondimensionalization scheme is used

$$\begin{gathered} Bi_1 = \frac{h_1 r_M}{k_1};\quad Bi_M(\tau) = \frac{h_M(t) r_M}{k_M};\quad \bar{Q}_i(\xi,\tau) = \frac{Q_i(r,t) r_M^2}{k_i T_{\mathrm{ref}}}; \\ \xi = \frac{r}{r_M},\quad \gamma_i = \frac{r_i}{r_M};\quad \tau = \frac{\alpha_1 t}{r_M^2};\quad \theta_{\mathrm{in}}(\xi) = \frac{T_{\mathrm{in}}(r)}{T_{\mathrm{ref}}}; \\ \theta_i(\xi,\tau) = \frac{T_i(r,t)}{T_{\mathrm{ref}}};\quad \delta_i = \frac{\alpha_i}{\alpha_1};\quad \kappa_i = \frac{k_i}{k_1};\quad p_i = \frac{k_i R_i}{r_M} \end{gathered} \tag{7}$$

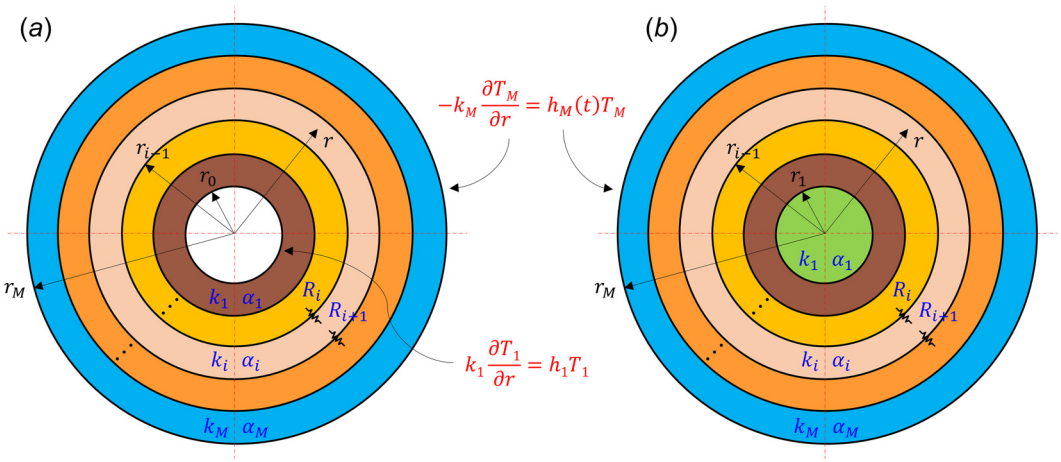

Fig. 1 Schematics of multilayer (*a*) annular and (*b*) solid cylinders, within which, thermal conduction with time-dependent convective heat transfer coefficients is analyzed in this work

where T_{ref} (K) is an arbitrary nonzero reference temperature.

Based on Eq. (7), the problem can be nondimensionalized to the following equations for the temperature field

$$\frac{1}{\delta_i}\frac{\partial \theta_i}{\partial \tau} = \frac{\partial^2 \theta_i}{\partial \xi^2} + \frac{1}{\xi}\frac{\partial \theta_i}{\partial \xi} + \bar{Q}_i(\xi,\tau) \tag{8}$$

$$\theta_i(\xi,\tau) = \theta_{in}(\xi) \quad (\tau = 0) \tag{9}$$

$$\frac{\partial \theta_1}{\partial \xi} = Bi_1\theta_1 \quad (\xi = \gamma_0) \tag{10}$$

$$-\frac{\partial \theta_M}{\partial \xi} = Bi_M(\tau)\theta_M \quad (\xi = 1) \tag{11}$$

$$\theta_{i-1}(\xi,\tau) = \theta_i(\xi,\tau) - p_i\frac{\partial \theta_i}{\partial \xi} \quad (\xi = \gamma_{i-1};\ i = 2,3,\ldots,M) \tag{12}$$

$$\kappa_{i-1}\frac{\partial \theta_{i-1}}{\partial \xi} = \kappa_i\frac{\partial \theta_i}{\partial \xi} \quad (\xi = \gamma_{i-1};\ i = 2,3,\ldots,M) \tag{13}$$

In order to proceed, the Biot number $Bi_M(\tau)$ is separated into two parts

$$Bi_M(\tau) = \sigma + F(\tau) \tag{14}$$

Here, $\sigma = Bi_M(0)$ is the Biot number at the initial time.

Inserting Eq. (14) in Eq. (11) results in

$$\frac{\partial \theta_M}{\partial \xi} + \sigma\theta_M = -F(\tau)\theta_M \quad (\xi = 1) \tag{15}$$

2.2.1 Shifting Function Method [25]. In order to solve Eqs. (8)–(10), (12)–(13), and (15), the following substitution is introduced [25,26,29]

$$\theta_i(\xi,\tau) = v_i(\xi,\tau) + f(\tau)g_i(\xi) \tag{16}$$

where $v_i(\xi,\tau)$, $g_i(\xi)$, and $f(\tau)$ are the transformed function, shifting function, and auxiliary function, respectively. $f(\tau)$ is given by

$$f(\tau) = -F(\tau)\theta_M(1,\tau) \tag{17}$$

Substituting Eq. (16) into Eqs. (8)–(10), (12), (13), and (15), and using Eq. (17) results in

$$\frac{1}{\delta_i}\left[\frac{\partial v_i}{\partial \tau} + f'g_i\right] = \frac{\partial^2 v_i}{\partial \xi^2} + f\left[g_i'' + \frac{1}{\xi}g_i'\right] + \frac{1}{\xi}\frac{\partial v_i}{\partial \xi} + \bar{Q}_i(\xi,\tau) \tag{18}$$

$$v_i(\xi,0) = \theta_{in}(\xi) \tag{19}$$

$$\left(\frac{\partial v_i}{\partial \xi}\right)_{\xi=\gamma_0} + fg_1'(\gamma_0) = Bi_1v_1(\gamma_0,\tau) + Bi_1fg_1(\gamma_0) \tag{20}$$

$$v_{i-1}(\gamma_{i-1},\tau) + fg_{i-1}(\gamma_{i-1}) = v_i(\gamma_{i-1},\tau) + fg_i(\gamma_{i-1}) - p_i\left[\left(\frac{\partial v_i}{\partial \xi}\right)_{\xi=\gamma_{i-1}} + fg_i'(\gamma_{i-1})\right] \tag{21}$$

$$\kappa_{i-1}\left[\left(\frac{\partial v_{i-1}}{\partial \xi}\right)_{\xi=\gamma_{i-1}} + fg_{i-1}'(\gamma_{i-1})\right] = \kappa_i\left[\left(\frac{\partial v_i}{\partial \xi}\right)_{\xi=\gamma_{i-1}} + fg_i'(\gamma_{i-1})\right] \tag{22}$$

$$\left(\frac{\partial v_M}{\partial \xi}\right)_{\xi=1} + \sigma v_M(1,\tau) + f\left[g_M'(1) + \sigma g_M(1)\right] = f \tag{23}$$

The shifting function $g_i(\xi)$ may be chosen in order to simplify Eqs. (18)–(23). Specifically, $g_i(\xi)$ may be designed in order to satisfy the following equations:

$$g_i'' = a \tag{24}$$

$$g_1'(\gamma_0) = Bi_1g_1(\gamma_0) \tag{25}$$

$$g_{i-1}(\gamma_{i-1}) = g_i(\gamma_{i-1}) - p_ig_i'(\gamma_{i-1}) \tag{26}$$

$$\kappa_{i-1}g_{i-1}'(\gamma_{i-1}) = \kappa_ig_i'(\gamma_{i-1}) \tag{27}$$

$$g_M'(1) = 1 \tag{28}$$

$$g_M(1) = 0 \tag{29}$$

Equation (24) has the following general solution [29]

$$g_i(\xi) = \frac{a}{2}\xi^2 + b_i\xi + c_i \tag{30}$$

where b_i and c_i are unknown coefficients to be determined. Equations (25)–(29) represent $(2M+1)$ linear algebraic equations in an equal number of unknowns, a, b_i, and c_i. A solution for the unknowns can be easily determined by using matrix inversion.

The substitution of Eq. (29) into Eq. (16) results in

$$\theta_M(1,\tau) = v_M(1,\tau) \tag{31}$$

Further, substituting Eqs. (17) and (24) into (18) and using Eq. (31) yields the following partial differential equation

$$\frac{\partial v_i}{\partial \tau} - \delta_i\frac{\partial^2 v_i}{\partial \xi^2} - \frac{\delta_i}{\xi}\frac{\partial v_i}{\partial \xi} - g_i(\xi)F(\tau)v_M'(1,\tau) + \left\{-g_i(\xi)F'(\tau) + \frac{\delta_i}{\xi}F(\tau)g_i'(\xi) + \delta_iaF(\tau)\right\}v_M(1,\tau) = \delta_i\bar{Q}_i(\xi,\tau) \tag{32}$$

The properties of the shifting function given by Eqs. (25)–(29) result in considerable simplification in Eqs. (20)–(23). The following equations may be obtained

$$\left(\frac{\partial v_1}{\partial \xi}\right)_{\xi=\gamma_0} = Bi_1v_1(\gamma_0,\tau) \tag{33}$$

$$v_{i-1}(\gamma_{i-1},\tau) = v_i(\gamma_{i-1},\tau) - p_i\left(\frac{\partial v_i}{\partial \xi}\right)_{\xi=\gamma_{i-1}} \tag{34}$$

$$\kappa_{i-1}\left(\frac{\partial v_{i-1}}{\partial \xi}\right)_{\xi=\gamma_{i-1}} = \kappa_i\left(\frac{\partial v_i}{\partial \xi}\right)_{\xi=\gamma_{i-1}} \tag{35}$$

$$\left(\frac{\partial v_M}{\partial \xi}\right)_{\xi=1} + \sigma v_M(1,\tau) = 0 \tag{36}$$

2.2.2 Orthogonal Expansion Method [14,30,31]. Equations (32), (19), and (33)–(36) admit the following general solution:

$$v_i(\xi,\tau) = \sum_{n=1}^{\infty}\psi_{i,n}(\xi)q_n(\tau) \tag{37}$$

where the functions $\psi_{i,n}(\xi)$ are the eigenfunctions, which may be written as

$$\psi_{i,n}(\xi) = \mu_{i,n}J_0(\beta_{i,n}\xi) + \eta_{i,n}Y_0(\beta_{i,n}\xi) \tag{38}$$

where

$$\beta_{i,n} = \sqrt{\frac{\delta_1}{\delta_i}}\lambda_n \tag{39}$$

and λ_n are the eigenvalues.

By requiring that the solution (37) satisfy the boundary conditions (33)–(36) and using Eq. (39), Eq. (38) may be expressed as follows [14]:

$$\psi_{i,n}(\xi) = \Phi_{i,n}(\lambda_n) X_{i,n}(\lambda_n, \xi) \tag{40}$$

where the functions $\Phi_{i,n}(\lambda_n)$ and $X_{i,n}(\lambda_n, \xi)$ are given by

$$\Phi_{1,n}(\lambda_n) = 1;\ \Phi_{i,n}(\lambda_n) = \varphi_i \varphi_{i-1} \ldots \varphi_3 \varphi_2 \ (i = 2, 3, \ldots, M) \tag{41}$$

$$X_{i,n}(\lambda_n, \xi) = J_0\left(\sqrt{\frac{\delta_1}{\delta_i}}\lambda_n \xi\right) + \Pi_{i,n}(\lambda_n) Y_0\left(\sqrt{\frac{\delta_1}{\delta_i}}\lambda_n \xi\right) \tag{42}$$

The functions φ_i appearing in equations above are

$$\varphi_i = \frac{X_{i-1,n}(\lambda_n, \gamma_{i-1})}{X_{i,n}(\lambda_n, \gamma_{i-1}) - p_i X'_{i,n}(\lambda_n, \gamma_{i-1})} \tag{43}$$

$$\varphi_M = \frac{\kappa_{M-1} X'_{M-1,n}(\lambda_n, \gamma_{M-1})}{\kappa_M X'_{M,n}(\lambda_n, \gamma_{M-1})} \tag{44}$$

The function $\Pi_{i,n}(\lambda_n)$ which explicitly appears in Eq. (42) is given by

$$\Pi_{1,n}(\lambda_n) = -\frac{Bi_1 J_0(\lambda_n \gamma_0) + \lambda_n J_1(\lambda_n \gamma_0)}{Bi_1 Y_0(\lambda_n \gamma_0) + \lambda_n Y_1(\lambda_n \gamma_0)} \tag{45}$$

$$\begin{aligned}
\Pi_{i,n}(\lambda_n) = -\Bigg[& \kappa_i \sqrt{\frac{\delta_1}{\delta_i}}\lambda_n J_1\left(\sqrt{\frac{\delta_1}{\delta_i}}\lambda_n \gamma_{i-1}\right) X_{i-1,n}(\lambda_n, \gamma_{i-1}) \\
& + \kappa_{i-1} J_0\left(\sqrt{\frac{\delta_1}{\delta_i}}\lambda_n \gamma_{i-1}\right) X'_{i-1,n}(\lambda_n, \gamma_{i-1}) \\
& + \kappa_{i-1} p_i \sqrt{\frac{\delta_1}{\delta_i}}\lambda_n J_1\left(\sqrt{\frac{\delta_1}{\delta_i}}\lambda_n \gamma_{i-1}\right) X'_{i-1,n}(\lambda_n, \gamma_{i-1}) \Bigg] \\
& \Big/ \Bigg[\kappa_i \sqrt{\frac{\delta_1}{\delta_i}}\lambda_n Y_1\left(\sqrt{\frac{\delta_1}{\delta_i}}\lambda_n \gamma_{i-1}\right) X_{i-1,n}(\lambda_n, \gamma_{i-1}) \\
& + \kappa_{i-1} Y_0\left(\sqrt{\frac{\delta_1}{\delta_i}}\lambda_n \gamma_{i-1}\right) X'_{i-1,n}(\lambda_n, \gamma_{i-1}) \\
& + \kappa_{i-1} p_i \sqrt{\frac{\delta_1}{\delta_i}}\lambda_n Y_1\left(\sqrt{\frac{\delta_1}{\delta_i}}\lambda_n \gamma_{i-1}\right) X'_{i-1,n}(\lambda_n, \gamma_{i-1}) \Bigg] \\
& (i = 2, 3, \ldots, M)
\end{aligned} \tag{46}$$

$$\begin{aligned}
\Pi_{M,n}(\lambda_n) = & -\left[\sigma J_0\left(\sqrt{\frac{\delta_1}{\delta_M}}\lambda_n\right) - \sqrt{\frac{\delta_1}{\delta_M}}\lambda_n J_1\left(\sqrt{\frac{\delta_1}{\delta_M}}\lambda_n\right)\right] \\
& \Big/ \left[\sigma Y_0\left(\sqrt{\frac{\delta_1}{\delta_M}}\lambda_n\right) - \sqrt{\frac{\delta_1}{\delta_M}}\lambda_n Y_1\left(\sqrt{\frac{\delta_1}{\delta_M}}\lambda_n\right)\right]
\end{aligned} \tag{47}$$

The eigenvalue λ_n may be obtained by recognizing that Eq. (46) with $i = M$ must yield the same expression as Eq. (47). This can be shown to result in

$$\begin{aligned}
& - \left[\kappa_M \sqrt{\frac{\delta_1}{\delta_M}}\lambda_n J_1\left(\sqrt{\frac{\delta_1}{\delta_M}}\lambda_n \gamma_{M-1}\right) X_{M-1,n}(\lambda_n, \gamma_{M-1})\right. \\
& + \kappa_{M-1} J_0\left(\sqrt{\frac{\delta_1}{\delta_M}}\lambda_n \gamma_{M-1}\right) X'_{M-1,n}(\lambda_n, \gamma_{M-1}) \\
& \left. + \kappa_{M-1} p_M \sqrt{\frac{\delta_1}{\delta_M}}\lambda_n J_1\left(\sqrt{\frac{\delta_1}{\delta_M}}\lambda_n \gamma_{M-1}\right) X'_{M-1,n}(\lambda_n, \gamma_{M-1})\right] / \\
& \left[\kappa_M \sqrt{\frac{\delta_1}{\delta_M}}\lambda_n Y_1\left(\sqrt{\frac{\delta_1}{\delta_M}}\lambda_n \gamma_{M-1}\right) X_{M-1,n}(\lambda_n, \gamma_{M-1})\right. \\
& + \kappa_{M-1} Y_0\left(\sqrt{\frac{\delta_1}{\delta_M}}\lambda_n \gamma_{M-1}\right) X'_{M-1,n}(\lambda_n, \gamma_{M-1}) \\
& \left. + \kappa_{M-1} p_M \sqrt{\frac{\delta_1}{\delta_M}}\lambda_n Y_1\left(\sqrt{\frac{\delta_1}{\delta_M}}\lambda_n \gamma_{M-1}\right) X'_{M-1,n}(\lambda_n, \gamma_{M-1})\right] \\
& - \left[\sigma J_0\left(\sqrt{\frac{\delta_1}{\delta_M}}\lambda_n\right) - \sqrt{\frac{\delta_1}{\delta_M}}\lambda_n J_1\left(\sqrt{\frac{\delta_1}{\delta_M}}\lambda_n\right)\right] / \\
& \left[\sigma Y_0\left(\sqrt{\frac{\delta_1}{\delta_M}}\lambda_n\right) - \sqrt{\frac{\delta_1}{\delta_M}}\lambda_n Y_1\left(\sqrt{\frac{\delta_1}{\delta_M}}\lambda_n\right)\right] = 0
\end{aligned} \tag{48}$$

Equation (48) represents the eigenequation, the roots of which may be computed to determine the eigenvalues. It can be shown that for the special case of equal properties in all layers, perfect thermal contact between layers and large Bi_1, Eq. (48) correctly reduces to Eq. (24) of Tu and Lee [26] who analyzed thermal conduction in a homogeneous annular cylinder with zero temperature on the inner surface. In fact, when all layers have uniform properties, $\Pi_{i,n}(\lambda_n)$ given by Eqs. (45)–(47) are identical. In other words, in this case, the eigenequation derived equating Eq. (46) with $i = M$ and Eq. (47) can also be obtained by simply Eqs. (45) and (47). Then, the eigenequation for the problem described by Tu and Lee [26] can be obtained by setting a very large value of Bi_1.

The eigenfunction $\psi_{i,n}(\xi)$ can be shown to satisfy the following orthogonality relation

$$\sum_{i=1}^{M} \frac{\kappa_i}{\delta_i} \int_{\gamma_{i-1}}^{\gamma_i} \xi \psi_{i,m}(\xi) \psi_{i,n}(\xi) d\xi = \begin{cases} 0 & m \neq n \\ N_n & m = n \end{cases} \tag{49}$$

where N_n represents the norm as follows:

$$N_n = \sum_{i=1}^{M} \frac{\kappa_i}{\delta_i} \int_{\gamma_{i-1}}^{\gamma_i} \xi \psi_{i,n}^2(\xi) d\xi \tag{50}$$

The integrals above may be evaluated as follows (see details in Appendix B in Ref. [14])

$$\int_{\gamma_{i-1}}^{\gamma_i} \xi \psi_{i,n}^2(\xi) d\xi = \left[\frac{\xi^2 \psi_{i,n}^2}{2}\right]_{\gamma_{i-1}}^{\gamma_i} + \left[\frac{\xi^2 \psi_{i,n}'^2}{2\lambda_n^2}\right]_{\gamma_{i-1}}^{\gamma_i} \tag{51}$$

where $i = 1, 2, \ldots, M$.

By using Eq. (37) in Eq. (32), the following equation may be derived

$$\sum_{n=1}^{\infty}\Bigg\{\psi_{i,n}(\xi)q_n'(\tau)-\delta_i\psi_{i,n}''(\xi)q_n(\tau)-\frac{\delta_i}{\xi}\psi_{i,n}'(\xi)q_n(\tau) -g_i(\xi)F(\tau)\psi_{M,n}(1)q_n'(\tau)\Big\} +\sum_{n=1}^{\infty}\Bigg\{-g_i(\xi)F'(\tau)+\frac{\delta_i}{\xi}F(\tau)g_i'(\xi)+\delta_i aF(\tau)\Bigg\} \psi_{M,n}(1)q_n(\tau)=\delta_i\bar{Q}_i(\xi,\tau) \tag{52}$$

In order to proceed, a series expansion of $\delta_i\bar{Q}_i(\xi,\tau)$ may be carried out as follows:

$$\delta_i\bar{Q}_i(\xi,\tau)=\sum_{n=1}^{\infty}\psi_{i,n}(\xi)\phi_n(\tau) \tag{53}$$

where $\phi_n(\tau)$ are functions to be determined. For each layer, Eq. (53) is multiplied by $\frac{\kappa_i}{\delta_i}\xi\psi_{i,n}(\xi)$ and integrated within each layer, followed by adding together equations for all layers. Based on the principle of quasi-orthogonality of eigenfunctions in a multilayer geometry, this results in

$$\phi_n(\tau)=\frac{1}{N_n}\sum_{i=1}^{M}\kappa_i\int_{\gamma_{i-1}}^{\gamma_i}\xi^*\bar{Q}_i(\xi^*,\tau)\psi_{i,n}(\xi^*)d\xi^* \tag{54}$$

where N_n is the norm given by Eq. (50).

Substituting the series expansion (53) for $\delta_i\bar{Q}_i(\xi,\tau)$ in Eq. (52) results in

$$\sum_{n=1}^{\infty}\Bigg\{\psi_{i,n}(\xi)q_n'(\tau)-\delta_i\psi_{i,n}''(\xi)q_n(\tau)-\frac{\delta_i}{\xi}\psi_{i,n}'(\xi)q_n(\tau) -g_i(\xi)F(\tau)\psi_{M,n}(1)q_n'(\tau)\Big\} +\sum_{n=1}^{\infty}\Bigg\{-g_i(\xi)F'(\tau)+\frac{\delta_i}{\xi}F(\tau)g_i'(\xi)+\delta_i aF(\tau)\Bigg\}\psi_{M,n}(1)q_n(\tau) =\sum_{n=1}^{\infty}\psi_{i,n}(\xi)\phi_n(\tau) \tag{55}$$

A term-by-term comparison in Eq. (55) results in

$$\psi_{i,n}(\xi)q_n'(\tau)-g_i(\xi)F(\tau)\psi_{M,n}(1)q_n'(\tau) -\delta_i\psi_{i,n}''(\xi)q_n(\tau)-\frac{\delta_i}{\xi}\psi_{i,n}'(\xi)q_n(\tau) +\Bigg\{-g_i(\xi)F'(\tau)+\frac{\delta_i}{\xi}F(\tau)g_i'(\xi)+\delta_i aF(\tau)\Bigg\}\psi_{M,n}(1)q_n(\tau) =\psi_{i,n}(\xi)\phi_n(\tau) \tag{56}$$

Now, for each i, Eq. (56) is multiplied by $\frac{\kappa_i}{\delta_i}\xi\psi_{i,n}(\xi)$, followed by integration from $\xi=\gamma_{i-1}$ to $\xi=\gamma_i$. The resulting expressions are added for $i=1,2,\ldots,M$, resulting in

$$q_n'(\tau)+\frac{\lambda_n^2-\omega_nF'(\tau)+\chi_nF(\tau)}{1-\omega_nF(\tau)}q_n(\tau)=\frac{\phi_n(\tau)}{1-\omega_nF(\tau)} \tag{57}$$

where

$$\omega_n=\frac{\psi_{M,n}(1)}{N_n}\sum_{i=1}^{M}\frac{\kappa_i}{\delta_i}\int_{\gamma_{i-1}}^{\gamma_i}\xi^*g_i(\xi^*)\psi_{i,n}(\xi^*)d\xi^* \tag{58}$$

$$\chi_n=\frac{\psi_{M,n}(1)}{N_n}\left[\sum_{i=1}^{M}\kappa_i\int_{\gamma_{i-1}}^{\gamma_i}g_i'(\xi^*)\psi_{i,n}(\xi^*)d\xi^*+a\sum_{i=1}^{M}\kappa_i\int_{\gamma_{i-1}}^{\gamma_i}\xi^*\psi_{i,n}(\xi^*)d\xi^*\right] \tag{59}$$

By substituting Eq. (37) into Eq. (19) and using the orthogonality relation, Eq. (49), one may obtain the associated initial condition for $q_n(\tau)$ as follows:

$$q_n(0)=\frac{1}{N_n}\sum_{i=1}^{M}\frac{\kappa_i}{\delta_i}\int_{\gamma_{i-1}}^{\gamma_i}\theta_{i,n}(\xi^*)\xi^*\psi_{i,n}(\xi^*)d\xi^* \tag{60}$$

Finally, the solution for $q_n(\tau)$ is derived by solving the ordinary differential Eq. (57)

$$q_n(\tau)=\exp\left(-\int_0^{\tau}\frac{\lambda_n^2-\omega_nF'(\tau^*)+\chi_nF(\tau^*)}{1-\omega_nF(\tau^*)}d\tau^*\right) \left\{q_n(0)+\int_0^{\tau}\frac{\phi_n(\zeta)}{1-\omega_nF(\zeta)}\exp\left(\int_0^{\zeta}\frac{\lambda_n^2-\omega_nF'(s)+\chi_nF(s)}{1-\omega_nF(s)}ds\right)d\zeta\right\} \tag{61}$$

Substituting Eqs. (17), (30), (31), (37), (40), and (42) back into Eq. (16) results in the nondimensional temperature of ith layer in the multilayer cylinder as follows:

$$\theta_i(\xi,\tau)=\sum_{n=1}^{\infty}q_n(\tau)\Bigg\{\Phi_{i,n}(\lambda_n)\left[J_0\left(\sqrt{\frac{\delta_1}{\delta_i}}\lambda_n\xi\right) +\Pi_{i,n}(\lambda_n)Y_0\left(\sqrt{\frac{\delta_1}{\delta_i}}\lambda_n\xi\right)\right] -F(\tau)\left(\frac{a}{2}\xi^2+b_i\xi+c_i\right)\Phi_{M,n}(\lambda_n) \left[J_0\left(\sqrt{\frac{\delta_1}{\delta_M}}\lambda_n\right)+\Pi_{M,n}(\lambda_n)Y_0\left(\sqrt{\frac{\delta_1}{\delta_M}}\lambda_n\right)\right]\Bigg\} \tag{62}$$

Note that while the expression for $q_n(\tau)$ derived above is quite extensive, its computation is relatively straightforward. Once the values of the nondimensional input parameters for a problem are known, parameters such as $\Phi_{i,n}$, $\Pi_{i,n}$, and $F(\tau)$ can be easily computed, based on definitions in preceding equations. These parameters are then inserted in Eq. (61) in order to determine the coefficients q_n as functions of time. When these parameters are available in functional form, these calculations, especially the evaluation of integrals appearing in Eq. (61) may be carried out symbolically. In contrast, if such data are available in numerical form, for example, discrete experimental data for the time-dependent convective heat transfer coefficient, such integration may necessarily need to be carried out numerically.

2.3 Solid Cylinder. The temperature field of a one-dimensional multilayer solid cylinder with time-dependent heat convective coefficients $h_M(t)$ in the outer surface can be easily obtained by simplifying the analysis for a one-dimensional multilayer annular cylinder presented above. Since the temperature field of an axisymmetric solid cylinder has zero slope at the center, therefore, both the governing equations and the solution methodology presented above are also applicable for a solid cylinder by using $h_1=0$ and $r_0=0$ in Eq. (3), and consequently, $Bi_1=0$ and $\gamma_0=0$ in Eqs. (10), (20), (25), and (33).

The temperature field of the multilayer solid cylinder is still expressed by Eq. (62) except for that of the first layer. By letting $i=1$ in Eqs. (38), (42), and (62), and using Eq. (41), one may obtain the temperature field of the first layer for the multilayer solid cylinder as follows

$$\theta_1(\xi,\tau)=\sum_{n=1}^{\infty}q_n(\tau)J_0(\lambda_n\xi)-\sum_{n=1}^{\infty}q_n(\tau)F(\tau)\left(\frac{a}{2}\xi^2+b_1\xi+c_1\right)\Phi_{M,n}(\lambda_n)\left[J_0\left(\sqrt{\frac{\delta_1}{\delta_M}}\lambda_n\right)+\Pi_{M,n}(\lambda_n)Y_0\left(\sqrt{\frac{\delta_1}{\delta_M}}\lambda_n\right)\right] \tag{63}$$

Note that the equivalent of Eq. (45) is not needed for the case of a solid multilayer cylinder.

3 Results and Discussion

3.1 ***Comparison* With Past *Work for Special Cases*.** Two specific special cases are considered, for which, the temperature field computed using results from Sec. 2 is compared against results available from past work as well as a standard theoretical solution.

The first case pertains to a three-layer annular cylinder considered by de Monte [14], in which, two constant convective heat transfer boundary conditions were assumed on the inner and outer surfaces. No internal heat generation and thermal contact resistance were considered. Compared to this past work, the present work represents a more generalized treatment of a multilayer geometry. In order to compare the results of the present work with [14] for the special case considered, results from the present work are simplified under the assumptions of zero heat generation rate and zero interlayer thermal contact resistance. Under these assumptions, according to the definition of nondimensional parameters in Ref. [14] and the present work, one may obtain $p_i=0\,(i=2,3)$, $\lambda_n=\beta_n/\gamma_0$, $\sigma=Bi_4/(\kappa_3\gamma_0)$, $\gamma_3=1$, $\delta_1=1$, $\gamma_0=1$. Therefore, after suitable manipulation, the coefficients $\Pi_{i,n}$ $(i=1,2,3)$ in Eqs. (45)–(47) may be shown to reduce to

$$\Pi_{1,n}(\lambda_n)=-(Bi_1J_0(\beta_n)+\beta_nJ_1(\beta_n))/(Bi_1Y_0(\beta_n)+\beta_nY_1(\beta_n)) \tag{64}$$

$$\Pi_{2,n}(\lambda_n)=-\left[\kappa_2/\sqrt{\delta_2}J_1\left(\beta_n\gamma_2/\sqrt{\delta_2}\right)\tilde{X}_{1,n}(\gamma_2)-J_0\left(\beta_n\gamma_2/\sqrt{\delta_2}\right)\Lambda_{1,n}(\gamma_2)\right]/\left[\kappa_2/\sqrt{\delta_2}Y_1\left(\beta_n\gamma_2/\sqrt{\delta_2}\right)\tilde{X}_{1,n}(\gamma_2)-Y_0\left(\beta_n\gamma_2/\sqrt{\delta_2}\right)\Lambda_{1,n}(\gamma_2)\right] \tag{65}$$

$$\Pi_{3,n}(\lambda_n)=-\left[Bi_4J_0\left(\beta_n\gamma_4/\sqrt{\delta_3}\right)-\beta_n\kappa_3/\sqrt{\delta_3}J_1\left(\beta_n\gamma_4/\sqrt{\delta_3}\right)\right]/\left[Bi_4Y_0\left(\beta_n\gamma_4/\sqrt{\delta_3}\right)-\beta_n\kappa_3/\sqrt{\delta_3}Y_1\left(\beta_n\gamma_4/\sqrt{\delta_3}\right)\right] \tag{66}$$

The eigenfunction given by Eq. (48) is simplified similarly to the following

$$\begin{aligned}&\left[\kappa_3/\sqrt{\delta_3}J_1\left(\beta_n\gamma_3/\sqrt{\delta_3}\right)\tilde{X}_{2,n}(\gamma_3)-\kappa_2/\sqrt{\delta_2}J_0\left(\beta_n\gamma_3/\sqrt{\delta_3}\right)\Lambda_{2,n}(\gamma_3)\right]\\&/\left[\kappa_3/\sqrt{\delta_3}Y_1\left(\beta_n\gamma_3/\sqrt{\delta_3}\right)\tilde{X}_{2,n}(\gamma_3)-\kappa_2/\sqrt{\delta_2}Y_0\left(\beta_n\gamma_3/\sqrt{\delta_3}\right)\Lambda_{2,n}(\gamma_3)\right]\\&-\left[Bi_4J_0\left(\beta_n\gamma_4/\sqrt{\delta_3}\right)-\beta_n\kappa_3/\sqrt{\delta_3}J_1\left(\beta_n\gamma_4/\sqrt{\delta_3}\right)\right]\\&/\left[Bi_4Y_0\left(\beta_n\gamma_4/\sqrt{\delta_3}\right)-\beta_n\kappa_3/\sqrt{\delta_3}Y_1\left(\beta_n\gamma_4/\sqrt{\delta_3}\right)\right]=0\end{aligned} \tag{67}$$

where the expressions of Bi_i $(i=1,4)$, β_n, γ_i $(i=2,3,4)$, $\tilde{X}_{i,n}(\gamma_{i+1})$ $(i=1,2)$ and $\Lambda_{i,n}(\gamma_{i+1})$ $(i=1,2)$ may be obtained from Ref. [14].

The above simplified formulas (45)–(48) are identical to equations (42*a*), (42*b*), (42*c*), and (40) in Ref. [14]. It should be noted that to explicitly compare the corresponding formulas between the present work and Ref. [14], Eqs. (45)–(47) are simplified using the relationship between nondimensional parameters in present work and [14].

The eigenequation derived above is identical to Eq. (40) of de Monte, showing that the present work results in identical eigenvalues as de Monte for the simplified, single-layer conditions considered in that work. Comparison of the predicted temperature distribution is also carried out for the above case, with $F(\tau)=0$, $Bi_M(\tau)=\sigma$ and $Q_i(r,t)=0$. Therefore, the general temperature distribution given by Eq. (62) reduces to

$$\theta_i(\xi,\tau)=\sum_{n=1}^{\infty}q_n(0)\exp\left(-\beta_n^2\tau\right)\Phi_{i,n}(\lambda_n)\left[J_0\left(\beta_n\xi/\sqrt{\delta_i}\right)+\Pi_{i,n}(\lambda_n)Y_0\left(\beta_n\xi/\sqrt{\delta_i}\right)\right] \tag{68}$$

where $q_n(0)$ is the same as c_n^+ with $m=n$ in Eq. (39) by de Monte [14] after corresponding manipulations. The temperature field for this special case based on the present work, given by Eq. (68) agrees exactly with the solution derived by de Monte [14] using the separation-of-variables method.

Comparison of the predicted temperature distribution is also carried out for a special case of constant convective heat transfer coefficient along with a nonhomogeneous initial condition. The solution to this problem was presented by Özışık [12]. In this case, $Bi_M(\tau)=\sigma$ and $Q_i(r,t)=0$. Therefore, $F(\tau)=0$ from Eqs. (7) and (14) and $\phi_n(\tau)=0$ from Eqs. (7) and (54). Therefore, the general solution given by Eq. (62) reduces to

$$\theta_i(\xi,\tau)=\sum_{n=1}^{\infty}q_n(0)\exp\left(-\lambda_n^2\tau\right)\Phi_{i,n}(\lambda_n)\left[J_0\left(\sqrt{\frac{\delta_1}{\delta_i}}\lambda_n\xi\right)+\Pi_{i,n}(\lambda_n)Y_0\left(\sqrt{\frac{\delta_1}{\delta_i}}\lambda_n\xi\right)\right] \tag{69}$$

where $q_n(0)$ is still given by Eq. (60).

Further, when all layers have the same properties and $Bi_1=\infty$, Eq. (69) can be simplified as

$$\theta(\xi,\tau)=\sum_{n=1}^{\infty}\frac{\exp\left(-\lambda_n^2\tau\right)}{N_n}\psi_n(\xi)\int_{\gamma_0}^{1}\theta_{in}(\xi^*)\xi^*\psi_n(\xi^*)d\xi^* \tag{70}$$

where

$$N_n=\int_{\gamma_0}^{1}\xi^*\psi_n^2(\xi^*)d\xi^* \tag{71}$$

$$\psi_n(\xi)=J_0(\lambda_n\xi)-\frac{J_0(\lambda_n\gamma_0)}{Y_0(\lambda_n\gamma_0)}Y_0(\lambda_n\xi) \tag{72}$$

The temperature field for this special case based on the present work, given by Eq. (70) agrees exactly with the solution derived by Özışık [12] using the integral transform method.

Finally, comparison with a previously reported special case of a two-layer solid cylinder with internal heat generation in both layers and constant convective heat transfer coefficient on the outer surface is carried out. This problem is a special case of the more generalized treatment in the present work. A solution for this special case has been derived in the past [32]. For the same set of parameters reported in this work ($\kappa_2=0.5$, $\delta_2=0.5$, $\gamma_1=0.5$, $\bar{Q}_1=5.0$, $\bar{Q}_2=2.0$, $Bi=10$), the temperature field is computed using the analytical model derived in the present work. A comparison between the two is presented in Fig. 2(*a*) in terms of nondimensional temperature as a

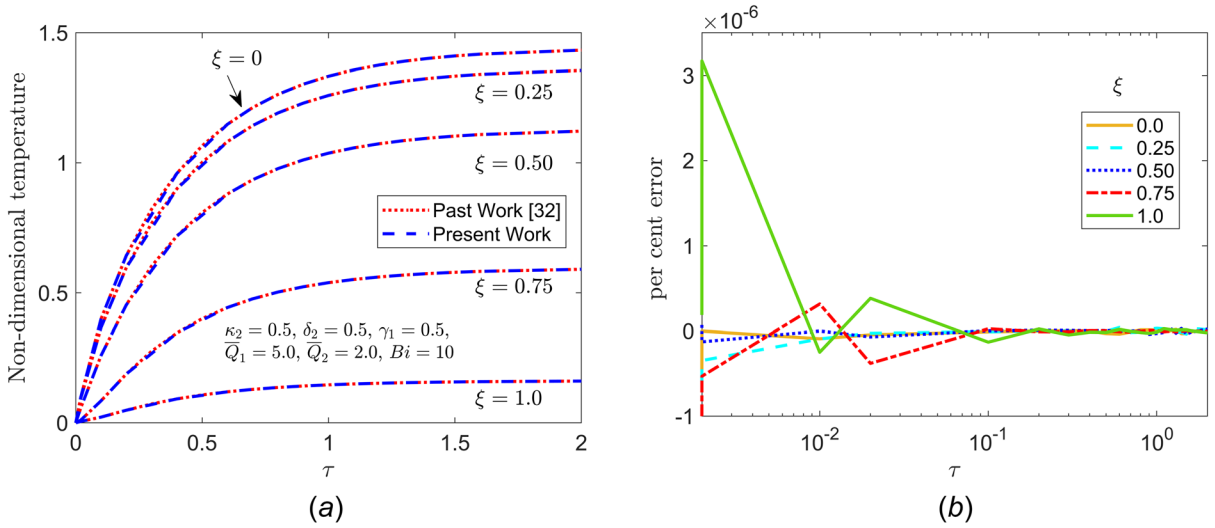

Fig. 2 Comparison of present work with past work [32] for a special case: (*a*) nondimensional temperature as a function of time at five different locations for a two-layer solid cylinder problem with internal heat generation and constant convective heat transfer coefficient on the outer boundary. Results from present work and past work are both plotted. (*b*) % error as a function of time at the five different locations considered in (*a*).

function of time at five different locations. Figure 2(*a*) shows excellent agreement between the two. The percent error between the two is plotted in Fig. 2(*b*), showing that the temperature fields computed from the two techniques are practically identical. Note that the differences in nondimensionalization schemes between the present work and past work are reconciled prior to the comparison presented in Fig. 2, in which, all nondimensional parameters correspond to the definitions in the present work.

Note that the comparisons discussed above do not necessarily establish the universal correctness of the time- and space-dependent temperature field derived here, but, nevertheless, provide verification for special cases that the general problem solved here may reduce to under certain conditions.

3.2 Comparison With Standard Analytical Solution. Another comparison is carried out with a special case, for which, an analytical solution is easily derivable independent of the present work. The problem considered is that of a single-layer annular cylinder with constant h_1 and h_M on the inner and outer surfaces, respectively, in addition to constant heat generation. For this special case, the temperature distribution can be readily derived using separation of variables technique and it is of interest to compare this with the general model presented above.

In this case, for the analytical solution derived in this work, one may substitute $F(\tau) = 0, \Phi_{i,n}(\lambda_n) = 1, i = 1$ and $\sqrt{\frac{\delta_1}{\delta_i}} = 1$ into Eq. (62), resulting in the following temperature distribution

$$\theta(\xi, \tau) = \sum_{n=1}^{\infty} \psi_n(\xi) q_n(\tau) \tag{73}$$

where

$$\psi_n(\xi) = J_0(\lambda_n \xi) - \frac{\lambda_n J_1(\lambda_n \gamma_0) + Bi_1 J_0(\lambda_n \gamma_0)}{\lambda_n Y_1(\lambda_n \gamma_0) + Bi_1 Y_0(\lambda_n \gamma_0)} Y_0(\lambda_n \xi) \tag{74}$$

Further, the substitution of $F(\tau) = 0, \Phi_{i,n}(\lambda_n) = 1, i = 1$, and $\sqrt{\frac{\delta_1}{\delta_i}} = 1$ in Eq. (62), followed by some mathematical manipulation results in the following expression for $q_n(\tau)$.

$$q_n(\tau) = q_n(0)\exp\left(-\lambda_n^2 \tau\right) + \frac{\bar{Q}\left(1 - \exp\left(-\lambda_n^2 \tau\right)\right)}{\lambda_n^2 N_n} \int_{\gamma_0}^{1} \xi^* \psi_n(\xi^*) d\xi^* \tag{75}$$

Finally, putting $\sigma = Bi_M$, $\sqrt{\frac{\delta_1}{\delta_M}} = 1$, and $M = 1$ into Eq. (47) and comparing the resulting expression with Eq. (45) can be shown to lead to the following eigenequation:

$$\begin{aligned} &J_1(\lambda_n\gamma_0)Y_1(\lambda_n)\lambda_n^2 + Bi_1 J_0(\lambda_n\gamma_0)Y_1(\lambda_n)\lambda_n \\ &\quad - Bi_M J_1(\lambda_n\gamma_0)Y_0(\lambda_n)\lambda_n - Bi_1 Bi_M J_0(\lambda_n\gamma_0)Y_0(\lambda_n) \\ &\quad - J_1(\lambda_n)Y_1(\lambda_n\gamma_0)\lambda_n^2 - Bi_1 J_1(\lambda_n)Y_0(\lambda_n\gamma_0)\lambda_n \\ &\quad + Bi_M J_0(\lambda_n)Y_1(\lambda_n\gamma_0)\lambda_n + Bi_1 Bi_M J_0(\lambda_n)Y_0(\lambda_n\gamma_0) = 0 \end{aligned} \tag{76}$$

The temperature distribution and eigenequation obtained above by simplifying the general results are identical to an independent derivation based on the separation of variables method for this special case, presented in Appendix A. Note that the integral appearing in Eq. (75) can be shown to be given by

$$\begin{aligned} \int_{\gamma_0}^{1} \xi^* \psi_n(\xi^*) d\xi^* &= \frac{J_1(\lambda_n) - \gamma_0 J_1(\lambda_n\gamma_0)}{\lambda_n} \\ &\quad - \frac{\lambda_n J_1(\lambda_n\gamma_0) + Bi_1 J_0(\lambda_n\gamma_0)}{\lambda_n Y_1(\lambda_n\gamma_0) + Bi_1 Y_0(\lambda_n\gamma_0)} \left(\frac{Y_1(\lambda_n) - \gamma_0 Y_1(\lambda_n\gamma_0)}{\lambda_n} \right) \end{aligned} \tag{77}$$

3.3 Effect of Number of Terms. The temperature distribution derived in this work is in the form of an eigenvalue-based series solution. Therefore, it is important to understand the convergence of this series and to determine how many eigenvalues must be used for a reasonable tradeoff between accuracy and computational cost. In order to investigate this in the context of the present problem, a representative three-layer problem is considered. Table 1 presents the values of various parameters used for this investigation. Figure 3 plots the temperature distribution in space and time for this problem computed with different number of eigenvalues. These plots show that the spatial temperature distribution, as well as variation in time, converges very quickly as the number of eigenvalues increases. While there is some deviation between curves corresponding to 1 and 5 eigenvalues, the curves corresponding to 5 and 10 eigenvalues are practically identical. This shows that, for the set of parameters considered here, only five eigenvalues are sufficient for good computational accuracy. Note that this is a useful insight since the general eigenequation for this problem is quite complicated and determining the eigenvalues may not be straightforward. However, it is good practice to repeat this exercise to examine the convergence of the series solution for the specific problem under consideration,

Table 1 Values of various parameters for a three-layer problem solved to demonstrate the capabilities of the analytical model

	Parameters					
Figure	M	r_i (mm) ($i = 0, 1, 2.. M$)	Q_i (kW/m^3)	k_i (W/(m·K))	α_i (mm^2/s)	h_1 (W/(m^2·K))
3	3	10, 20, 30, 40	400, 200, 600	1, 2, 3	1, 2, 4	1000
4(a)	3	10, 20, 30, 40	400, 200, 600	1, 2, 3	1, 2, 4	1000
4(b), 5(b)	4	0,10, 20, 30, 40	400, 200, 600, 500	1, 2, 3, 4	1, 2, 4, 3	—
5(a)	3	10, 20, 30, 40	400, 200, 600	1, 2, 3	1, 2, 4	250
6	3	10, 20, 30, 40	600, 600, 600	2, 2, 2	2, 2, 2	500
7	3	10, 20, 30, 40	600, 300, 900	1, 2, 3	1, 2, 4	1000

especially considering the time domain in which the computation of temperature is to be carried out. A general eigenvalue convergence and error analysis for the present work is mathematically difficult due to the complicated nature of the eigenequation and other results and is outside the scope of the present work. Please note that here, eigenvalues are obtained numerically by successively implementing the Newton Raphson method in regions where the eigenequation changes sign, and then zooming in, so as to determine the roots of the eigenequation within the region with increasingly finer accuracy. The width of the region is taken to be thin enough so as not to miss roots that may be potentially located very close to each other.

3.4 Effect of Time-Dependent Convective Heat Transfer Coefficient. The influence of various forms of the time-dependent convective heat transfer coefficient on the temperature distribution is investigated next. Linear, sinusoidal, and step function forms of the time-dependent convective heat transfer coefficient are considered, as these are some of the most commonly encountered variations with time observed in practical problems. For example, sinusoidal functions are investigated in problems with inherent periodic variation, such as alternating currents or periodic changes in heat transfer due to blade rotation in turbomachinery [33]. Step functions may be appropriate in scenarios involving abrupt on/off action, such as actuation of a switch/valve, or coolant flow failure. For example, failure of coolant flow in a nuclear reactor may be modeled as a step-function in $h(t)$, where $h(t)$ is a large value due to forced flow until the time of failure, and, later, $h(t)$ is a much lower value due to natural convection alone after the time of failure [34]. Finally, linear functions may be appropriate in other applications where the boundary conditions change in a slower, controlled fashion. For example, thermal loading of an optical fiber has been modeled as a combination of linear and sinusoidal functions for the time-dependent convective heat transfer coefficients [35]. Unsteady cooling of thermoelectric devices has also been modeled with a linear convective heat transfer coefficient [36]. Similar linear functions have been extracted from experimental temperature measurements [37] and have been used in analytical heat transfer models for flow boiling over a heated tube [20].

A linear convective heat transfer coefficient profile, given by $Bi_M(t) = A + B \cdot t$ is considered first. For a fixed value of A, Fig. 4 plots the temperature on the outer surface of a multilayer cylinder as a function of time for different values of the slope B. Results pertaining to a three-layer annular cylinder and a four-layer solid cylinder are presented in Figs. 4(*a*) and 4(*b*), respectively. As expected, these plots show that the temperature increases at first, due to the onset of heat generation in the various layers. Since the value of B is non-negative in each case, therefore, $Bi_M(t)$ increases with time, resulting in greater cooling with increasing time. This results in the temperature profile reaching a peak at a certain time and then decaying away due to more and more effective cooling. As expected, the peak temperature reached is larger for smaller values of B. In addition, the peak also occurs at greater times for small B, as it takes longer for the convective cooling effect to dominate over heat generation.

The case of sinusoidal convective heat transfer coefficient is investigated next. For a representative profile $Bi_M(t) = Bi_{M,0}(1 + \cos(\omega t))$, Fig. 5 plots the transient temperature on the outer surface of a multilayer cylinder for different values of ω, while the amplitude is held constant. Cases for annular and solid cylinder are presented in Figs. 5(*a*) and 5(*b*), respectively. Curves presented in these figures are found to be consistent with the frequency of the convective heat transfer coefficient for both annular and solid cylinders. The peak temperature attained is highest for the smallest frequency. This is because the smaller the frequency of the function $Bi_M(t)$, the longer is the residence time of the function $Bi_M(t)$ around its minimum. In other words, the cooling effect of the largest period of the function $Bi_M(t)$ near its minimum is the worst. Similarly, the smaller the frequency of the function $Bi_M(t)$, the longer the residence time of the function $Bi_M(t)$ around the maximum.

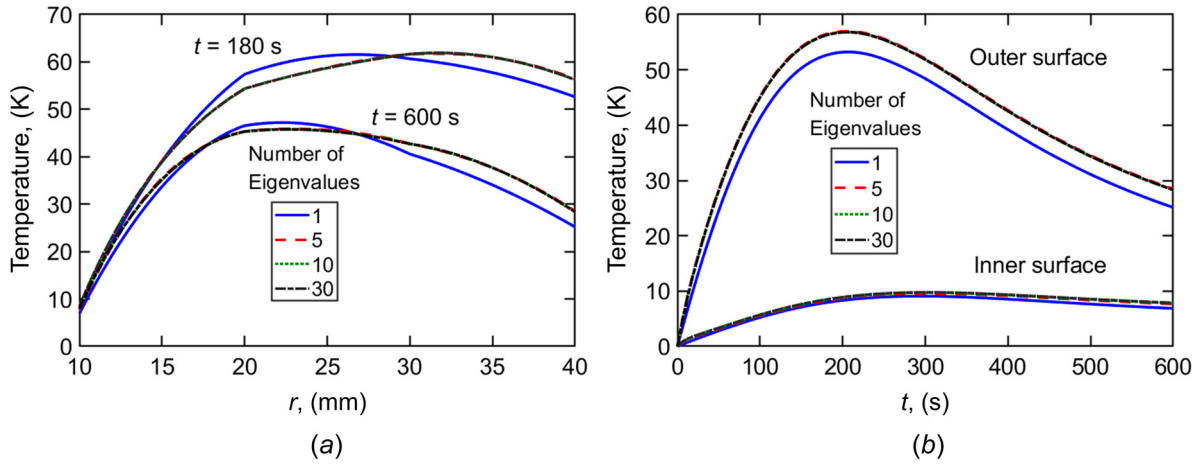

Fig. 3 Effect of number of eigenvalues considered: (*a*) *T* versus *r* at two different times, (b) *T* versus *t* at two different locations plotted for 1, 5, 10, and 30 eigenvalues. Here, $h_M(t)=400t/t_0$ W/(m^2·K), where $t_0=1000$ (m^2·K·s)/W, and other parameters are listed in Table 1.

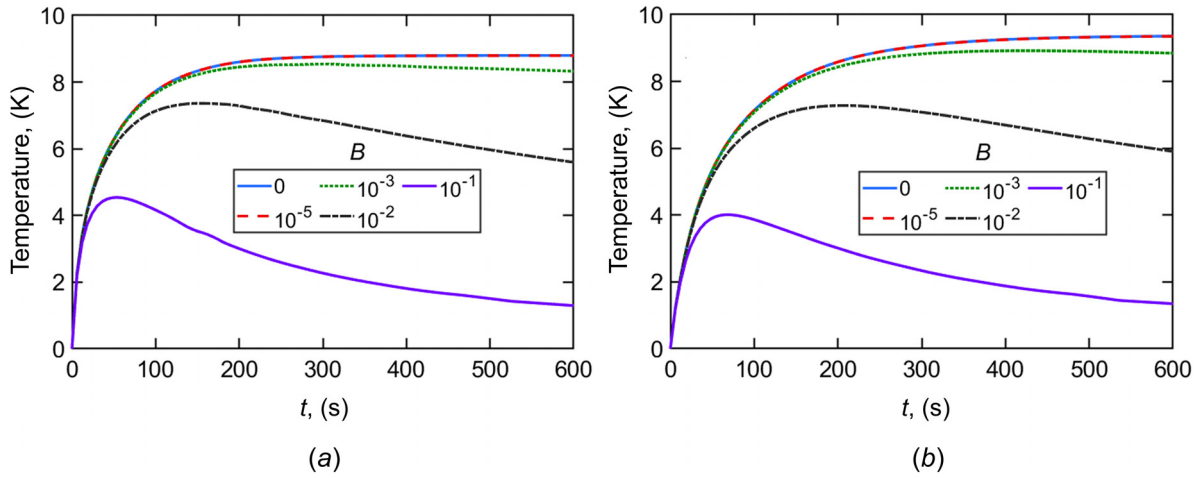

Fig. 4 Effect of linear $Bi_M(t) = A + Bt$: Temperature on the outer surface of (*a*) an annular three-layer cylinder and (*b*) a four-layer solid cylinder as a function of time for different values of the slope *B*, with *A* = 10. Problem parameters are given in Table 1.

Finally, a step function convective heat transfer coefficient is considered. The Biot number on the outer boundary is assumed to change from $Bi_{M,1}$ to $Bi_{M,2}$ at $t = t_1$. For fixed value of $Bi_{M,1}$, Fig. 6 plots the temperature profiles at two different locations of an annular cylinder for different values of $Bi_{M,2}$, including $Bi_{M,2} = 0$, which corresponds to adiabatic conditions. Both plots show, as expected, the same temperature distribution regardless of the value of $Bi_{M,2}$ up to $t = t_1$, since $Bi_{M,1}$ is fixed. Afterwards, the temperature distribution varies, with the highest temperature rise obtained for the worst-case value of $Bi_{M,2} = 0$, in which case, there is no convective heat transfer on the outer surface at all. As $Bi_{M,2}$ increases, the temperature profile beyond $t = t_1$ shifts downwards, and, in the case of $Bi_{M,2} = 10$, there is no additional temperature rise, as an equilibrium is maintained between heat generation and convective heat removal.

3.5 Effect of Thermal Contact Resistance. The impact of thermal contact resistance between adjacent layers is investigated next. For the case of a three-layer annular cylinder, the impact of accounting for R_2 and R_3, the contact resistances between layers 1 and 2, and layers 2 and 3, respectively is presented in Fig. 7. While Fig. 7(*a*) compares the case of contact resistance with perfect contact, Fig. 7(*b*) presents results for different values of the contact resistance. These plots show, as expected, smooth temperature distributions for the case of perfect thermal contact, whereas there are discontinuities at the interface whenever the thermal contact resistance is nonzero. In Fig. 7(*a*), the temperature rise for the case of contact resistance is greater than the perfect contact case for layers 1 and 2, whereas, there is a small reduction in temperature due to contact resistance for layer 3. This can be explained on the basis of the different heat generation rates in the three layers, with heat generation in layer 3 being the largest. In general, layer 2 appears to be the hottest, which is likely because it is farthest away from either of the two cooling boundaries while still generating appreciable heat.

Moreover, Fig. 7(*a*) shows greater impact of thermal contact resistance between layers 2 and 3, than between layers 1 and 2. In order to investigate this further, temperature plots for a number of thermal contact resistance combinations are presented in Fig. 7(*b*). These plots demonstrate that thermal contact resistance between the first two layers has only a weak impact on the temperature field. For example, there is negligible change in the temperature curve at $R_2 = 0.005\ \mathrm{Km^2/W}$ compared to the perfect contact baseline. Even for a relatively large value of $R_2 = 0.5\ \mathrm{Km^2/W}$, the interfacial temperature jump is quite small. In comparison, thermal contact resistance between the two outer layers causes a much larger jump in

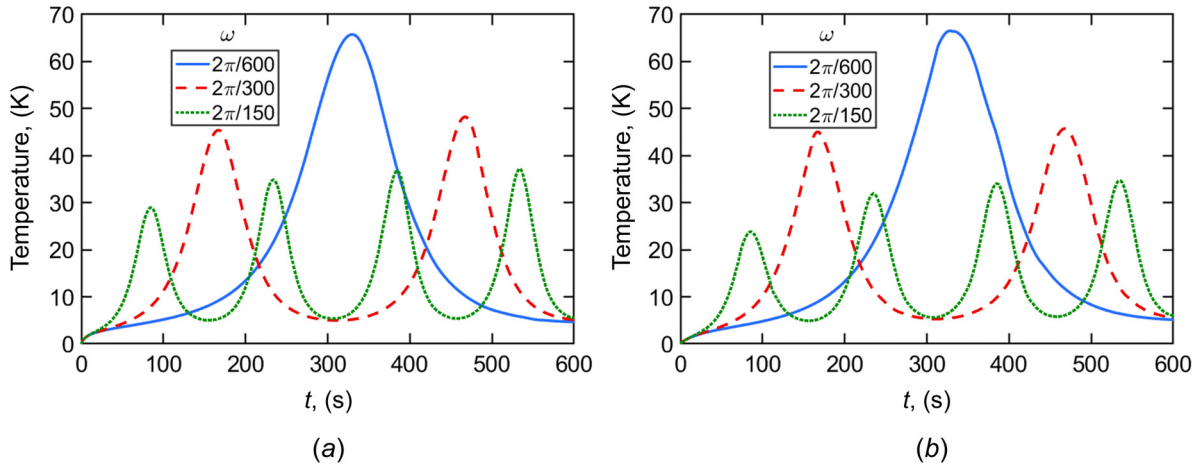

Fig. 5 Effect of sinusoidal $Bi_M(t) = Bi_{M,0}(1 + \cos(\omega t))$, $Bi_{M,0} = 10$: Temperature on the outer surface of (*a*) an annular three-layer cylinder and (*b*) a four-layer solid cylinder as a function of time for different values of frequency ω. Problem parameters are given in Table 1.

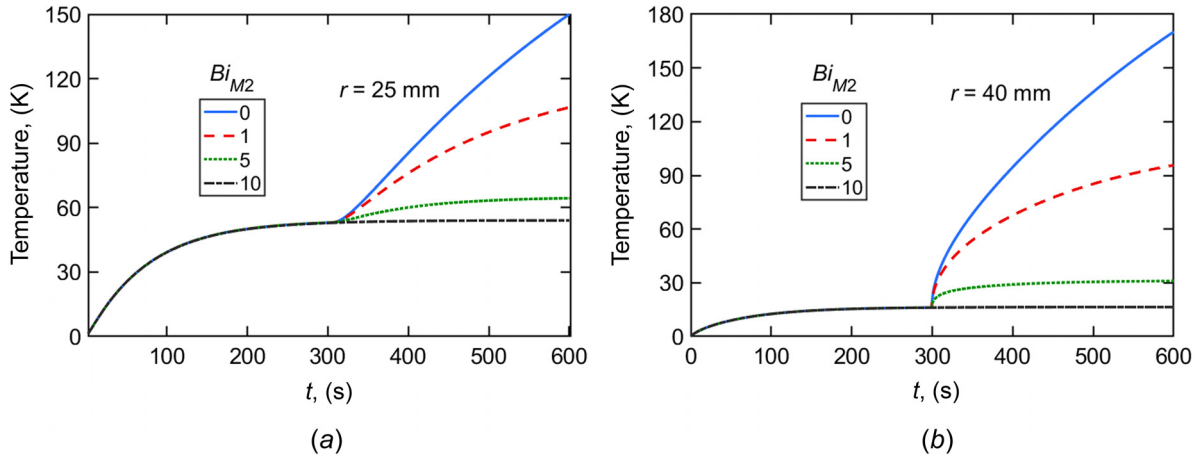

Fig. 6 Effect of step function $Bi_M(t)=Bi_{M,1}$ if $0<t<t_1$, and $Bi_{M,2}$ otherwise: Temperature at (*a*) center of the second layer and (*b*) outer surface of the three-layer body as functions of time for different values of $Bi_{M,2}$. Problem parameters are given in Table 1. Additionally, $t_1=300$ s, $t_2=600$ s, $h_1=500$ W/(m^2·K), and $Bi_{M,1}=10$.

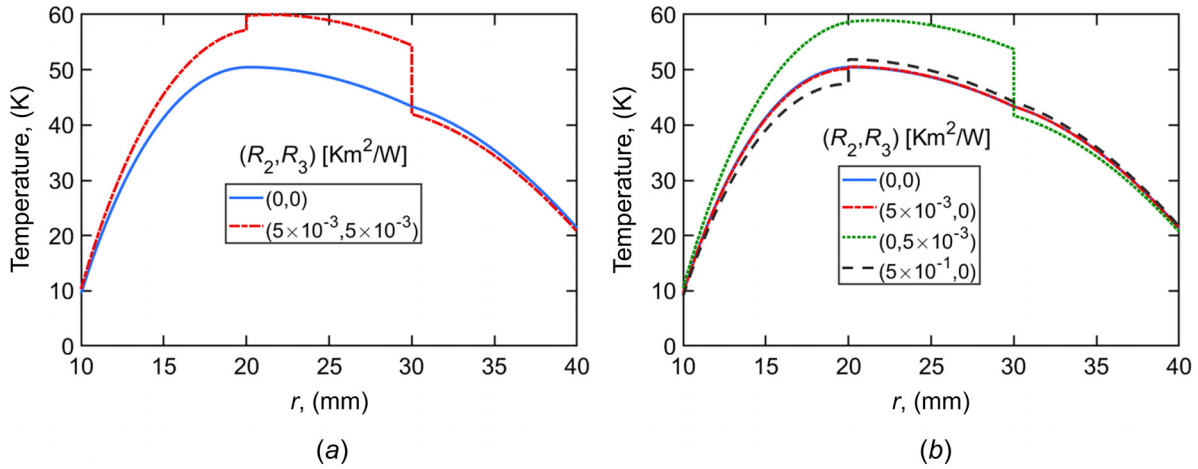

Fig. 7 Effect of interlayer thermal contact resistances R_2 and R_3 in a three-layer problem: Temperature at $t=600$ s as functions of location for different values of R_2 and R_3. Here, $h_M(t)=800t/t_0$ W/(m^2·K), where $t_0=1000$ (m^2·K·s)/W, and other parameters are given in Table 1.

the temperature curve, even for relatively small value. As shown in Fig. 7(*b*), the analytical model enables evaluation and comparison of various such combinations of parameter values.

4 Conclusions

The key novelty of the present work is in the development of a theoretical model that accounts for one-dimensional multilayer cylindrical thermal conduction in the presence of time-dependent convective heat transfer coefficient on the outer boundary. While cases with constant or even spatially varying convective heat transfer have been addressed before, accounting for time-dependent convective heat transfer coefficient is a lot more complicated. The present work generalizes past papers that solved only specific problems and, as expected, results from the present work correctly reduce to past results for these special cases. Further, the good agreement with numerical simulations also increases confidence in the model presented here.

The present work assumes axisymmetric conditions. While circumferential variation can, in principle, be accounted for, a vast majority of problems of engineering interest are axisymmetric in nature. Further, this work assumes that all properties and parameters other than the convective heat transfer coefficient on the outer surface are constant and uniform. This is also a reasonable assumption for most engineering problems, especially when the temperature rise is reasonably small.

This work contributes toward an improved understanding of multilayer thermal conduction. By accounting for time-dependent convective heat transfer coefficient, the model may accurately address a number of practical engineering problems where such variation in time occurs.

Funding Data

- Key Scientific and Technological Breakthroughs of Henan Province (Grant No. 222102520007).

Data Availability Statement

The datasets generated and supporting the findings of this article are obtainable from the corresponding author upon reasonable request.

Declarations of Competing Interests

None.

Nomenclature

a, b, c = coefficients in equation (30)
Bi = Biot number
f = auxiliary function

F = dimensionless time function
g = shifting function
h = convective heat transfer coefficient, $\mathrm{W{\cdot}m^{-2}{\cdot}K^{-1}}$
k = thermal conductivity, $\mathrm{W{\cdot}m^{-1}{\cdot}K^{-1}}$
p = dimensionless thermal contact resistance
q = dimensionless time-variable function
Q = heat generation rate, $\mathrm{W{\cdot}m^{-3}}$
$\bar{Q}$ = dimensionless heat generation rate
r = space coordinate, m
R = thermal contact resistance, $\mathrm{K{\cdot}m^2{\cdot}W^{-1}}$
t = time, s
T = temperature, K
v = transformed function

Greek Symbols

α = thermal diffusivity, $\mathrm{m^2s^{-1}}$
γ = geometric ratio
δ = thermal diffusivity ratio
θ = dimensionless temperature
κ = thermal conductivity ratio
λ = eigenvalue
ξ = dimensionless space coordinate
σ = initial value of $Bi_M(\tau)$
τ = dimensionless time
ψ = eigenfunction

Subscripts

i = layer number
in = initial state
m, n = integer numbers
ref = reference

Appendix A: Separation of Variables Based Solution for Special Case in Sec. 3.2

This Appendix briefly presents a derivation of the solution for the transient temperature distribution for the special case of uniform heat generation in a single-layer annular cylinder with constant h_1 and h_M on the inner and outer surfaces, respectively, with which, the general model presented in this work is compared.

For this problem, based on the separation of variables technique, a general solution for the transient temperature distribution may be written as

$$\theta(\xi,\tau)=\sum_{n=1}^{\infty}\psi_n(\xi)q_n(\tau) \tag{A1}$$

where $\psi_n(\xi)$ are eigenfunctions, which, for the cylindrical problem are given by a linear combination of zeroth order Bessel functions of the first and second kind, i.e., $\psi_n(\xi)=J_0(\lambda_n\xi)+c_nY_0(\lambda_n\xi)$. Now, using the convective boundary condition at the inner surface, it may be shown that $c_n=-\frac{\lambda_nJ_1(\lambda_n\gamma_0)+Bi_1J_0(\lambda_n\gamma_0)}{\lambda_nY_1(\lambda_n\gamma_0)+Bi_1Y_0(\lambda_n\gamma_0)}$, and, further, using the convective boundary condition at the outer surface, the following eigenequation may be derived:

$$\begin{aligned}&J_1(\lambda_n\gamma_0)Y_1(\lambda_n)\lambda_n^2+Bi_1J_0(\lambda_n\gamma_0)Y_1(\lambda_n)\lambda_n\\&\quad-Bi_MJ_1(\lambda_n\gamma_0)Y_0(\lambda_n)\lambda_n-Bi_1Bi_MJ_0(\lambda_n\gamma_0)Y_0(\lambda_n)\\&\quad-J_1(\lambda_n)Y_1(\lambda_n\gamma_0)\lambda_n^2-Bi_1J_1(\lambda_n)Y_0(\lambda_n\gamma_0)\lambda_n\\&\quad+Bi_MJ_0(\lambda_n)Y_1(\lambda_n\gamma_0)\lambda_n+Bi_1Bi_MJ_0(\lambda_n)Y_0(\lambda_n\gamma_0)=0\end{aligned} \tag{A2}$$

This leaves the unknown coefficients $q_n(\tau)$ to be determined. This is carried out by following the method of undetermined parameters. Briefly, Eq. (A1) is differentiated with respect to time, followed by substitution of the transient derivative with spatial derivatives using the governing energy equation. The resulting equation is multiplied by the eigenfunction $\psi_m(\xi)$, followed by integration from $\xi=\gamma_0$ to $\xi=1$. Mathematical manipulation, including the use of the boundary conditions may be shown to result in the following expression for $q_n(\tau)$

$$q_n(\tau)=q_n(0)\exp\left(-\lambda_n^2\tau\right)+\frac{\bar{Q}\left(1-\exp\left(-\lambda_n^2\tau\right)\right)}{\lambda_n^2N_n}\int_{\gamma_0}^{1}\xi^*\psi_n(\xi^*)d\xi^* \tag{A3}$$

This completes the derivation of the solution for this special case, independent of the general method presented in this work.

References

[1] Kandlikar, S. G., 2014, "Review and Projections of Integrated Cooling Systems for Three-Dimensional Integrated Circuits," ASME J. Electron. Packag., **136**(2), p. 024001.
[2] French, H., 1981, *Heat Transfer and Fluid Flow in Nuclear Systems*, 1st ed., Pergamon Press, Oxford, UK.
[3] Prikhod'ko, I. M., 1972, "Thermal Conductivity of a Two-Layer Wall for a Time-Varying Heat-Transfer Coefficient and Ambient Temperature," J. Eng. Phys, **18**, pp. 239–242.
[4] Daryabeigi, K., 2002, "Thermal Analysis and Design Optimization of Multilayer Insulation for Reentry Aerodynamic Heating," J. Spacecr. Rockets, **39**(4), pp. 509–514.
[5] Bhargava, A., Chanmugam, A., and Herman, C., 2014, "Heat Transfer Model for Deep Tissue Injury: A Step Towards an Early Thermographic Diagnostic Capability," Diagn. Pathol., **9**(1), pp. 36:1–18.
[6] Ferragut, L., Asensio, M. I., Cascón, J. M., Prieto, D., and Ramírez, J., 2013, "An Efficient Algorithm for Solving a Multi-Layer Convection-Diffusion Problem Applied to Air Pollution Problems," Adv. Eng. Software, **65**, pp. 191–199.
[7] Jain, A., McGinty, S., Pontrelli, G., and Zhou, L., 2022, "Theoretical Modeling of Endovascular Drug Delivery Into a Multilayer Arterial Wall From a Drug-Coated Balloon," Int. J. Heat Mass Transfer, **187**, p. 122572.
[8] Choobineh, L., Jones, J., and Jain, A., 2017, "Experimental and Numerical Investigation of Inter-Die Thermal Resistance in 3D ICs," ASME J. Electron. Packag., **139**, p. 020908.
[9] Oprins, H., Cherman, V., Vandevelde, B., Van der Plas, G., Marchal, P., and Beyne, E., 2012, "Numerical and Experimental Characterization of the Thermal Behavior of a Packaged DRAM-on-Logic Stack," IEEE 62nd Electronic Components and Technology Conference (ECTC), San Diego, CA, May 29-June 1, pp. 1081–1088.
[10] Sekar, D., 2008, "A 3D-IC Technology With Integrated Microchannel Cooling," International Interconnect Technology Conference, Burlingame, CA, June 1-4, pp. 13–15.
[11] Mikhailov, M. D., and Özışık, M. N., 1994, *Unified Analysis and Solutions of Heat and Mass Diffusion*, Dover Publications, New York.
[12] Özışık, M. N., 2013, *Boundary Value Problems of Heat Conduction*, Dover Publications, Mineola, NY.
[13] Yener, Y., and Özışık, M. N., 1974, "On the Solution of Unsteady Heat Conduction in Multi-Region Media With Time-Dependent Heat Transfer Coefficient," Proceedings of fifth International Heat Transfer Conference, Tokyo, Japan, Sept. 3-7, pp. 188–192.
[14] de Monte, F., 2002, "An Analytic Approach to Be Unsteady Heat Conduction Processes in One-Dimensional Composite Media," Int. J. Heat Mass Transfer, **45**(6), pp. 1333–1343.
[15] Choobineh, L., and Jain, A., 2015, "An Explicit Analytical Model for Rapid Computation of Temperature Field in a Three-Dimensional Integrated Circuit (3D IC)," Int. J. Therm. Sci., **87**, pp. 103–109.
[16] Choobineh, L., and Jain, A., 2012, "Analytical Solution for Steady-State and Transient Temperature Field in Vertically Integrated Three-Dimensional Integrated Circuits (3D ICs)," IEEE Trans. Compon., Packag. Manuf. Technol., **2**(12), pp. 2031–2039.
[17] Zhou, L., Parhizi, M., and Jain, A., 2021, "Theoretical Modeling of Heat Transfer in a Multilayer Rectangular Body With Spatially-Varying Convective Heat Transfer Boundary Condition," Int. J. Therm. Sci., **170**, p. 107156.
[18] Zhou, L., Parhizi, M., and Jain, A., 2021, "Analytical Solution for Temperature Distribution in a Multilayer Body With Spatially-Varying Convective Heat Transfer Boundary Condition on Both Ends," ASME J. Heat Mass Transfer-Trans. ASME, **143**(3), p. 034501.
[19] Zhou, L., Parhizi, M., and Jain, A., 2021, "Temperature Distribution in a Multi-Layer Cylinder With Circumferentially-Varying Convective Heat Transfer Boundary Conditions," Int. J. Therm. Sci., **160**, p. 106673.
[20] Thompson, J. J., and Holy, Z. J., 1969, "Axisymmetric Thermal Response Problems for a Spherical Fuel Element With Time Dependent Heat Transfer Coefficients," Nucl. Eng. Des., **9**(1), pp. 29–44.
[21] Al-Haddad, A. A., and Al-Binally, N., 1989, "Prediction of Heat Transfer Coefficient in Pulsating Flow," Int. J. Heat Fluid Flow, **10**(2), pp. 131–133.
[22] J. H., Lienhard, V., 1995, "Liquid Jet Impingement," Annu. Rev. Heat Transfer, **6**(6), pp. 199–270.
[23] Becker, N. M., Bivins, R. L., Hsu, Y. C., Murphy, H. D., White, A. B., Jr., and Wing, G. M., 1983, "Heat Diffusion With Time-Dependent Convective Boundary Condition," Int. J. Numer. Methods Eng., **19**(12), pp. 1871–1880.

[24] Lyubov, B. Y., and Yalovoi, N. I., 1969, "Heat Conductivity of a Body With Variable Heat Exchange Coefficient," J. Eng. Phys., **17**(4), pp. 1264–1270.
[25] Chen, H. T., Sun, S. L., Huang, H. C., and Lee, S. Y., 2010, "Analytic Closed Solution for the Heat Conduction With Time-Dependent Heat Convection Coefficient at One Boundary," Comput. Model. Eng. Sci., **59**, pp. 107–126.
[26] Tu, T. W., and Lee, S. Y., 2015, "Analytical Solution of Heat Conduction for Hollow Cylinders With Time-Dependent Boundary Condition and Time-Dependent Heat Transfer Coefficient," J. Appl. Math., **2015**, pp. 1–9.
[27] Özışık, M. N., and Murray, R. L., 1974, "On the Solution of Linear Diffusion Problems With Variable Boundary Condition Parameters," ASME J. Heat Mass Transfer-Trans. ASME, **96**(1), pp. 48–51.
[28] Il'chenko, O. T., 1973, "Temperature Field of a Two-Layered Plate With Time-Varying Heat-Transfer Conditions," J. Eng. Phys., **19**, pp. 1567–1570.
[29] Chiba, R., 2018, "An Analytical Solution for Transient Heat Conduction in a Composite Slab With Time-Dependent Heat Transfer Coefficient," Math. Prob. Eng., **2018**, pp. 1–11.
[30] Haji-Sheikh, A., and Beck, J. V., 1994, "Green's Function Solution for Thermal Wave Equation in Finite Bodies," Int. J. Heat Mass Transfer, **37**(17), pp. 2615–2626.
[31] Hays-Stang, K. J., and Haji-Sheikh, A., 1999, "A Unified Solution for Heat Conduction in Thin Films," Int. J. Heat Mass Transfer, **42**(3), pp. 455–465.
[32] Haji-Sheikh, A., "R0C11B3T00G11, Temperature and Heat Flux Solutions in Two-Layer Concentric Solid Cylinders With a Convective Surface and Prescribed Volumetric Heat Sources," Exact Analytical Conduction Toolbox, accessed Sept. 9, 2023, https://exact.unl.edu/
[33] Kartashov, E. M., 2019, "Heat Conduction at a Variable Heat-Transfer Coefficient," High Temp., **57**(5), pp. 663–670.
[34] Onyango, T. T. M., Ingham, D. B., Lesnic, D., and Slodička, M., 2009, "Determination of a Time-Dependent Heat Transfer Coefficient From Non-Standard Boundary Measurements," Math. Comput. Simul., **79**(5), pp. 1577–1584.
[35] Borukhov, V. T., and Kostyukova, O. I., 2013, "Identification of Time-Dependent Coefficients of Heat Transfer by the Method of Suboptimal Stage-by-Stage Optimization," Int. J. Heat Mass Transfer, **59**, pp. 286–294.
[36] Yang, Y. C., Chu, S. S., and Chang, W. J., 2004, "Thermally Induced Optical Effects in Optical Fibers by Inverse Methodology," J. Appl. Phys, **95**(9), pp. 5159–5165.
[37] Mori, M., and Kondo, M., 1993, "Temperature and Thermal Stress Analysis in a Structure With Uncertain Heat Transfer Boundary Conditions," Trans. JSME Ser. A, **59**(562), pp. 1514–1518.